



# An improved hair removal algorithm for dermoscopy images

Sezin Barın<sup>1</sup> · Gür Emre Güraksın<sup>2</sup>

Received: 1 February 2023 / Revised: 18 April 2023 / Accepted: 29 May 2023 /

Published online: 16 June 2023

© The Author(s), under exclusive licence to Springer Science+Business Media, LLC, part of Springer Nature 2023

## Abstract

Dermoscopy is commonly used for diagnosing skin cancer in its early stages. However, hair structures in dermoscopy images can negatively affect diagnosis. A proposed algorithm based on conventional image processing methods removes hair structures from these images. Removing hair structures is crucial for constructing accurate computer-aided diagnosis systems for skin cancer. To eliminate hair structures from dermoscopy images, a hair removal algorithm based on conventional image processing methods has been proposed in this study. The proposed algorithm was compared to the existing hair removal algorithms in literature and tested on the ISIC2018 dataset using the AlexNet architecture. The effects on computer-aided systems were assessed by training on images with and without hair. Results show that the algorithm performs well in removing hairs compared to previous studies and improves classification performance. Upon comparison with other literature studies, the recommended algorithm has exhibited consistently high performance, usually ranking among the top two performers in the rank analysis. Additionally, the integration of the suggested algorithm has led to improvements in the performance metrics of the AlexNet architecture, with increases of 0.9% in accuracy, 1.4% in sensitivity, 0.6% in specificity, and 1.06 in F1 score. The performance of the suggested algorithm indicates its potential as a practical and effective tool in clinical settings.

**Keywords** Image processing · Skin cancer · Hair removal algorithm · Deep learning

## 1 Introduction

In addition to being the most prevalent cancer type, skin cancer is also, depending on its kind and early diagnosis, the most curable cancer type [25, 27]. Due to the anatomy of skin cancers, there are two primary types: melanoma and non-melanoma skin cancer. Melanoma makes up only 1% of all skin cancers, yet it has a higher propensity

---

✉ Sezin Barın  
sbarin@aku.edu.tr

<sup>1</sup> Engineering Faculty, Biomedical Engineering Department, Afyon Kocatepe University, Afyonkarahisar, Turkey

<sup>2</sup> Engineering Faculty, Computer Engineering Department, Afyon Kocatepe University, Afyonkarahisar, Turkey

to develop and spread than other forms. The mortality rate is increased as a result. Although non-melanoma skin cancer types basal and squamous cells are the most frequently diagnosed, the numbers for these cancers are unknown. Since non-melanoma patients are exempt from reporting requirements to the cancer registry [35]. This is due to the fact that cases of non-melanoma skin cancer are classified as non-life threatening [6]. However, when we look at the studies on all cancer cases, about 4% of cases with excellent prognosis develop nodal metastases, and in 1.5% of the cases death from the disease is observed [19]. This shows that while the death rate from the more common non-melanoma skin cancer is lower, non-melanoma skin cancer can cause more deaths. Moreover, even though non-melanoma skin cancer patients have a low mortality rate from the condition, its serious consequences on people's quality of life should not be disregarded [8, 13].

Skin cancers can be diagnosed using a variety of imaging techniques, such as dermoscopy, confocal laser scanning microscopy, ultrasound, MRI, and PET. Since alternative methods cannot be employed, especially in the diagnosis of early-stage skin cancer, dermoscopy represents the primary and most preferred treatment [36]. It can be evaluated with the naked eye, though. Depending on the specialist's level of knowledge, these assessments can be subjective, error-prone, and time-consuming. Misdiagnoses can result in unfavorable outcomes including death, financial loss, or a decline in quality of life [14]. Dermoscopy, the initial method of investigation for diagnosis, morphological complications render the diagnosis process quite complicated. Computer aided solutions have proliferated in recent years in an effort to address these drawbacks of conventional diagnostic techniques and to aid specialists [3, 16, 20]. In addition to supporting experts, Computer aided systems (CAD) facilitate and accelerate the transition from diagnosis to diagnosis and increase the reliability of results. CAD generally consist of four stages: Preprocessing, segmentation, feature extraction and classification [32, 33]. Each step is strongly impacted by the success of the one before it. Therefore, in the literature, it is quite common to apply morphological image processing methods to remove noise or segment the relevant region in images that will be used in the training of deep learning architectures for computer-aided diagnostic systems [9, 12, 29, 43, 44]. One of the most pertinent elements that adversely affects the performance of CADs instantly includes morphological disorders of dermoscopy images [33]. In particular, hair structures that are not removed before dermoscopy imaging create an image on skin lesions and even cover the entire lesion. It is intimidating to identify the lesion boundary regions during the segmentation stage due to these hair formations [1], which negatively affect the features that will represent the classes in the feature extraction stage, reducing the performance of the classification stage due to incorrect decisions. In Fig. 1, sample images containing morphological hair images found in dermoscopy images have been given.

The presented issues have been attempted to be resolved in the literature by proposing various hair removal algorithms. Table 1 provides a summary of the studies conducted for removing hair structures in dermoscopy images. As shown in the table, the

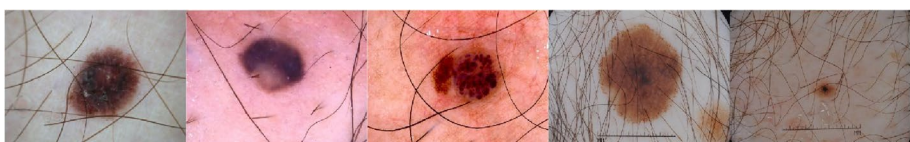


**Fig. 1** Morphological hair images found in dermoscopy images [10, 40]

**Table 1** The summarized literature methods related to hair removal in dermoscopy images

Work/Research	Year	Hair Removal Method	Inpainting Method	Dataset	Colour Space	Method
DullRazor [24]	1997	Morphological closing	Bilinear interpolation	-	RGB	Morphological
Xie et al. [41]	2009	Top-hat operator	PDE based method	40 images	RGB	Morphological
E-shaver (Kiani et al.) [21]	2011	Prewitt edge detector	Colour averaging	50 images	Gray Scale	Morphological
Abbas et al. [1]	2011	Derivative of Gaussian	Fast marching method	100 images	CIELab	Morphological
Toossi et al. [39]	2013	Adaptive Canny edge detector	Multiresolution coherence transport	50 images	Gray Scale	Morphological
Huang et al. [18]	2013	Multiscale matched	Median filtering	20 images	RGB, CIELab	Morphological
Xie et al. [42]	2015	Adaptive threshold	-	125 images	RGB, CIELab	Morphological
Koehoorn et al. [22]	2016	Multiscale skeletons	Fast marching method	300 images	HSV, RGB	Morphological
Bibiloni et al. [7]	2017	Soft color top-hat transforms	Soft color morphology operators	PH2 dataset	CIELab	Morphological
Ramella [33]	2021	Top-hat operator	regionfill	PH2 dataset, ISIC2016, NH13-data	HSV, RGB	Morphological
Attia et al. [5]	2019	Auto-encoder (12 convolution layer)	ISIC2017-345 images		RGB	Deep Learning
Talavera-Martinez et al. [38]	2020	Auto-encoder (10 convolution+2 recurrent layer)	-	PH2, dermquest, dermis, EDRA2002, ISIC	RGB	Deep Learning
Li et.al. [26]	2021	U-Net	Gated Convolution and SN-Patch GAN	ISIC2018-306 görüntüü	RGB	Deep Learning

existing studies can be examined in two stages: traditional image processing-based methods [1, 7, 18, 21, 24, 33, 39, 41] and deep learning-based methods [5, 26, 38].

Studies conducted using traditional image processing methods generally consist of two stages, which are the detection of hair structures and image inpainting. It can be seen that systems based on morphological closing [7, 33, 41] and opening [24] methods are more frequently preferred for the detection of hair structures. In addition to these, the other morphological image processing methods used in hair detection are the Derivative Gaussian[1], adaptive threshold [42], multiscale matched [18], multiscale skeletons [22], and edge detection algorithms such as Prewitt [21] and Canny [39]. Different methods such as bilinear interpolation [24], PDE (partial differential equation)-based method [41], color averaging [21], fast marching [1, 22], Multiresolution coherence transport [39], median filtering [18], Soft color morphology operators [7], and region-fill [33] have been used for inpainting on hair structures.

Observing the algorithms created with deep learning methods, it can be seen that most of them use architectures based on the auto-encoder structure [4, 26, 38]. Deep learning-based systems are observed to be more successful than the compared traditional image processing methods [1, 7, 18, 24, 39, 41]. In addition, deep learning-based hair removal methods may not require extra algorithms to inpaint the identified hair structures.

According to recent studies, deep learning techniques are more effective than conventional ones at solving the hair removal issue [5, 26, 38]. As a result, this approach will make it much easier for specialists to assess structures with their unaided eyes. Moreover, deep learning techniques have gained favor in most CAD systems in recent years due to the successful segmentation and classification processes. A new deep learning architecture will, however, significantly raise the computational cost of the system in the current scenario, merely for the hair removal problem. As a result, in order to use the CAD systems that will be established, extremely sophisticated and thus expensive technology will be required. Because of these factors, it may be more feasible to create a successful hair removal algorithm using traditional image processing methods. The lack of a dataset of original dermoscopy images with ground truth tags and segmented hair areas seems to be another drawback. Thus, in deep learning-based studies, artificial hair images are added, or studies are carried out on data sets that have removed hair structures with traditional image processing methods. This limits its application in the real-world scenario.

Since conventional image processing techniques can highlight specific details in algorithms, it is clear from applied studies that the top-hat algorithm based on the closure method is used frequently. The top-hat algorithm has, however, come under fire for its failure to recognize hairs that are close to the background. Examining the literature studies' findings reveals that there are problems with identifying weak, light-colored hairs in particular. In this study, a hair removal algorithm based on traditional image processing methods has been proposed in the light of these identified problems and deficiencies.

Two stages—hair detection and inpainting—make up the proposed hair removal algorithm. The red(R) channel, which is the color channel where the hairs in the images are most noticeable, is utilized during the phase of distinguishing the hairs. First, the top-hat operator is used in the hair detection step to make the details on the red channel clearer. Later, distinct morphological techniques are employed to create weak, thin hairs for the areas where the operator is inadequate in accentuating the detail. The thresholding algorithm based on the Otsu formula then was employed to segment the hairs as well. After removing the segmented areas other than the hair, the filling process based on the interpolation method was applied and the hairs were removed at the optimum level. For the evaluation of the method, in addition to the qualitative evaluation, quantitative parameters

such as MSE, PSNR, SSIM and MSSIM, which are used in similar studies, were also used. Meanwhile, the effectiveness of deep learning techniques using raw and hair-removed images was also compared at the same time.

The main contributions of this work are as follows:

1. Proposed a new hair removal algorithm based on the top-hat algorithm enhanced with flat-field correction and local brightening techniques.
2. Ranked proposed algorithm among the top performing hair removal algorithms compared to existing methods when evaluated with image quality metrics.
3. Applied the proposed hair removal algorithm to dermoscopy images and use deep learning for skin cancer classification, resulting in an average improvement of 1% in evaluation metrics.

The remainder of the article is organized in the following manner: The steps of the indicated hair removal procedure are outlined in Chapter 2 along with the datasets used. The evaluation of the suggested method's quantitative and qualitative outcomes, as well as comparisons with other studies, are covered in Chapter 3. An overall assessment of the study is provided in Chapter 4.

## 2 Material and method

This research proposes a technique to eliminate hair images on skin lesions in dermoscopy pictures using conventional image processing techniques. Figure 2 depicts the suggested hair removal algorithm's flowchart. The AlexNet architecture hair removal algorithm was also implemented and trained independently with raw images as part of the ongoing investigation in order to assess the impact of the suggested algorithm on the effectiveness of the classification studies to be produced using deep learning techniques.

### 2.1 Data set

In order to assess the suggested method, various image sets were deployed. The ISIC2018 [10, 40] data set, the most often used dermoscopy data set in the literature, was employed for the study's first testing. The ISIC2018 dataset comprises of 10,015 dermoscopy images, of which 1113 are melanoma, 6705 are melanocytic nevus, 514 are basal cell carcinoma, 327 are actinic keratoses, 1099 are benign keratoses, 115 are dermatofibromas, and 142 are vascular lesions. It is clear that there is a very uneven distribution of data among the classes. In this study, the classification success of the proposed hair removal algorithm on skin cancer process was carried out with AlexNet deep learning architecture. Therefore, the distribution of classes in the dataset is balanced. Because of this, data from the melanocytic nevus class were decreased to 1200 by lowering the data, while data from other classes were increased and guaranteed to have comparable quantities. Table 2 lists the quantity of data for each type. The data was augmented using reflection, rotation, blurring, and various hue, saturation, brightness, and contrast modifications. The proposed hair remove algorithm was implemented to this newly formed data set to train the AlexNet deep learning architecture, and performance results were compared to those obtained by training AlexNet with raw images. Since the

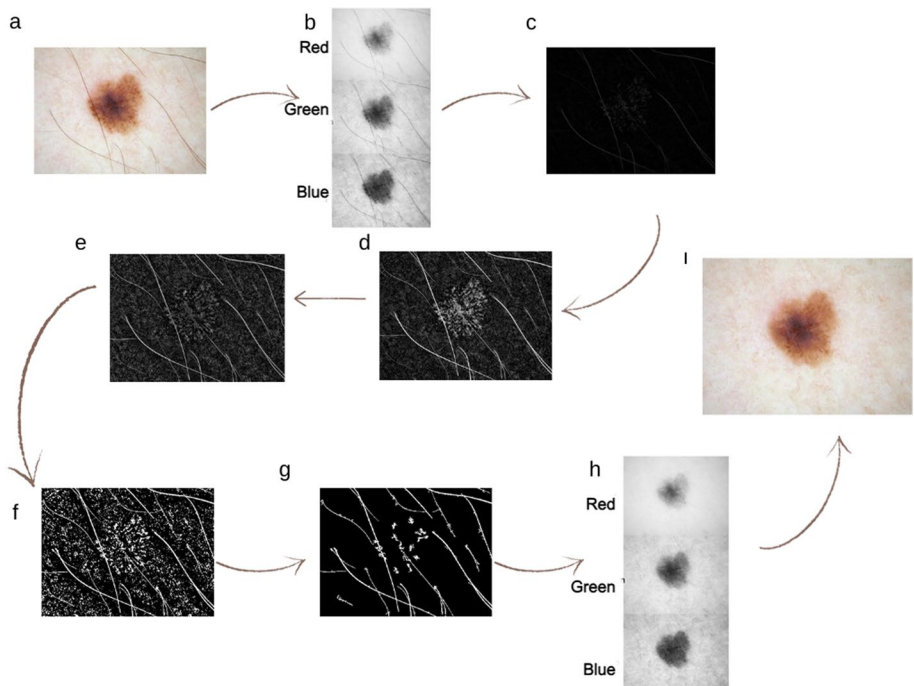


**Fig. 2** Flow Chart of Hair Removal Algorithm **a** Original Image, **b** Choosing Red channel from RGB channel, **c** Top-Hat Transform, **d** Local Brighting, **e** Flat-Field Correction, **f** Thresholding, **g** Opening small areas, **h** Inpainting, **i** Result

ISIC2018 data set did not contain distinct test and training data, a tenfold cross validation method was utilized. In each fold, 10% of the data was used for training, 10% for validation, and 80% for training.

To compare the hair removal algorithm with other studies, the H13GAN and H13SIM datasets, which were presented as open source in [15], were also included in the study in addition to ISIC2018. Thus, quantitative and qualitative comparisons were carried out between the images produced using the algorithms presented in the research [1, 7, 18, 24, 33, 39, 41] and the images produced using the suggested method.

**Table 2** Data distribution of ISIC 2018 data set with data reduction and increase applied by classes

Type of Skin Cancer	Number of Images
Melanoma	1113
Melanocytic nevus	1200
Basal cell carcinoma	1028
Actinic keratosis	981
Benign keratosis	1099
Dermatofibroma	575
Vascular lesion	710

## 2.2 Proposed hair removal algorithm

The suggested hair removal algorithm may be categorized into two basic constituents: hair extraction and inpainting. Figure 2 contains the proposed algorithm's flow diagram. The images were initially adjusted to make them all the same size. The gray-level images of red (R), green (G), and blue (B) channels were then quantitatively reviewed. Instances of dermoscopy images in the R-G-B channels are illustrated in Fig. 3. The R channel was utilized to segment the hair structures since it was the color channel that displayed the most obvious difference between the hair structures and the lesions.

After selecting the red color channel, where the hairs are most prominent, the top-hat operator was used, which is quite functional in detecting contrasting objects on non-uniform backgrounds [41]. There are two types of top-hat operators: white top-hat, which can detect bright structures, and black top-hat, which can detect dark structures. In the white top-hat operator (Eq. 5), morphological image operations, erosion (Eq. 2), and opening (Eq. 3) are applied in sequence to the image, and the resulting image is subtracted from the original image [45]. In the black top-hat operator (Eq. 6), morphological image operations, dilation (Eq. 1), and closing (Eq. 4) are applied in sequence to the image, and the original image is subtracted from the resulting image [45]. Mathematically, these can be expressed as follows (f:image, b:structuring element,  $f \oplus b$ :dilation,  $f \ominus b$ : erosion,  $f \circ b$ : opening,  $f \bullet b$ :closing);

$$f \oplus b(x, y) = \underbrace{\max}_{u, v} (f(x - u), y - v) + b(u, v) \quad (1)$$

$$f \ominus b(x, y) = \underbrace{\min}_{u, v} (f(x + u), y + v) - b(u, v) \quad (2)$$

$$f \circ b(x, y) = (f \ominus b) \oplus b \quad (3)$$

$$f \bullet b(x, y) = (f \oplus b) \ominus b \quad (4)$$

$$\text{white top - hat}(x, y) = f(x - y) - f \circ b(x, y) \quad (5)$$

$$\text{black top - hat}(x, y) = f \bullet b(x, y) - f(x - y) \quad (6)$$

In this study, the black top-hat operator was used, which performs the filling operation because the hair structures are darker than the rest of the image. A dermoscopy R channel view with the top-hat operator applied has been supplied in Fig. 4b. In the TopHat filtering process, a disc with a radius of 10 was used as a structural filter element.

Figure 4b shows that the top-hat operator was not sufficient to accurately identify and characterize the hair structures present in the image. To address this issue, local lighting was used to enhance the details and brighten the darkly lit sections. This operator illuminates dark areas at a predetermined rate to bring out more detail. Figure 4c shows an example image that was produced using the local brightening method.

Digital images often contain flaws due to noise sources. One commonly used method in such cases is the flat-field correction (FFC) algorithm. The FFC algorithm corrects image imperfections caused by changes in detector sensitivity per pixel and optical path

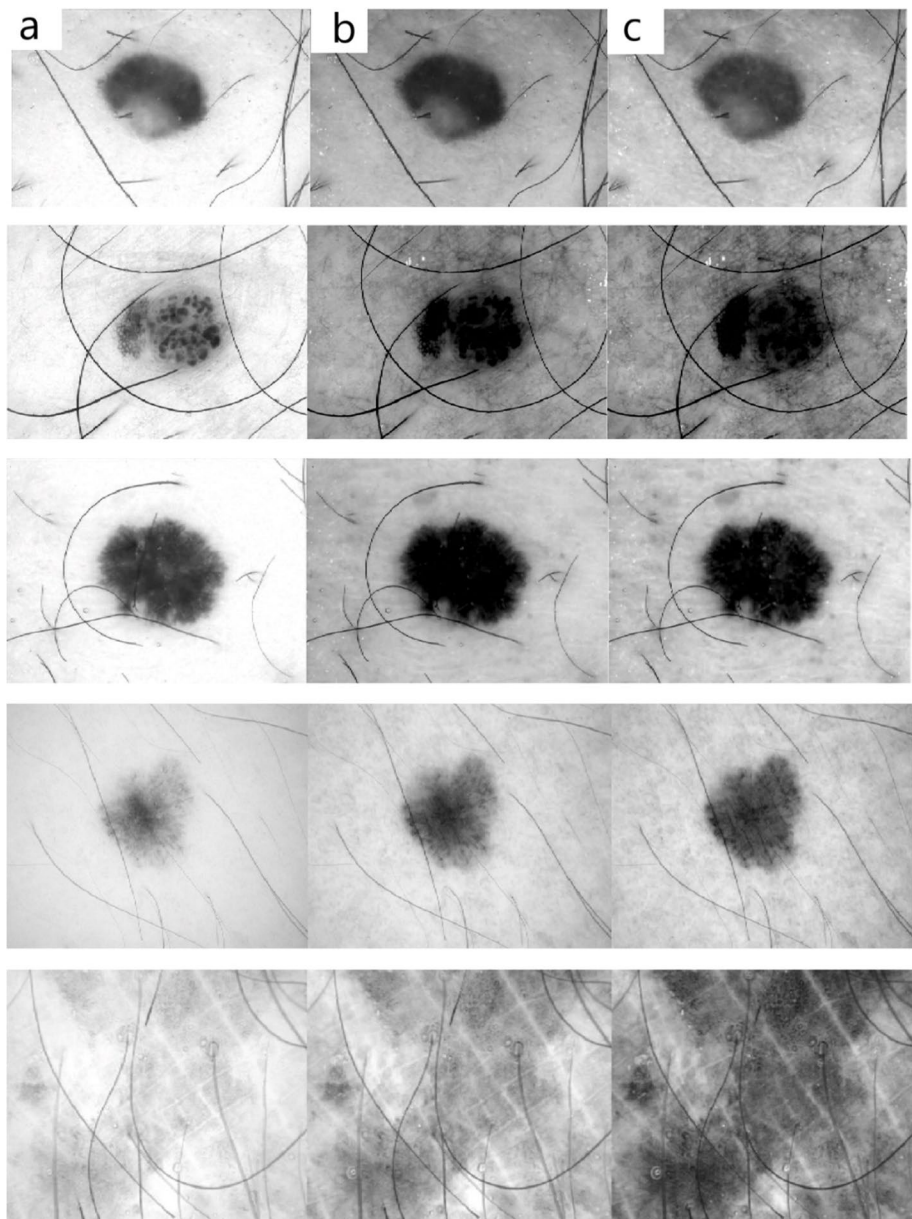


**Fig. 3** RGB color layers of sample skin lesion images **a** Red Channel, **b** Green Channel, **c** Blue Channel

distortions [11]. This algorithm equalizes the background of the image and removes the intensity of each object from position-dependent shading effects. In the FFC algorithm, the noise sources in the images are assumed to be the same, obtained from the same image source. Therefore, the correction process is applied using an offset image( $I_o$ ) obtained from the images taken from the same source and a dark field image( $I_d$ ) [34]. In

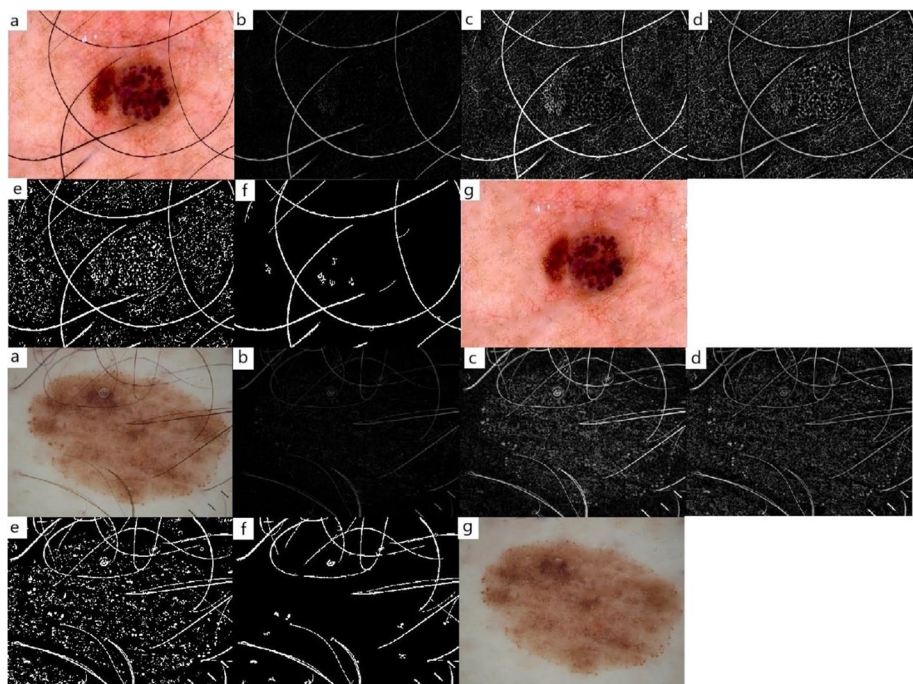


**Fig. 4** Hair removal algorithm steps on the sample skin lesion image **a** Original image, **b** Top-hat algorithm applied image, **c** Locally illuminated image, **d** Image obtained with Flat-field correction, **e** Image obtained with Otsu threshold, **f** Wiping out small parts, **g** Output of hair removal algorithm

skin lesion images, some areas of the image may be different in brightness due to irregular lighting and perception [30] (usually, the center is brighter). However, since the images used in the study were not taken from a fixed imaging source, the offset image was obtained by applying a Gaussian filter generated with the standard deviation value in the correction process. FFC can be expressed mathematically, as stated in the Eq. 7. Figure 4d shows an exemplar of a flat area correction-generated image

( $I$ =corrected image,  $I_r$ =raw image,  $I_o$ =flat field image,  $I_d$ =dark frame,  $m$ =image-averaged value of ( $F-D$ ))

$$I = \frac{(I_r - I_d)xm}{I_o - I_d} \quad (7)$$

Once each aspect of the image has been made clear, a threshold must be specified before the image can be converted to binary format. One of the highest quality techniques for figuring out threshold has been used in this process: the Otsu approach. The Otsu approach determines the foreground and background as though each pixel value in the image is a threshold value, and foreground and background weight, mean, and variance values are calculated [31]. The goal is to determine the threshold value at which the total foreground and background spread are at the lowest. Using the threshold value determined by the Otsu method, the gray format image is converted to binary format. An example of the image converted to binary format with the Otsu method is given in Fig. 4e.

Following the Otsu method's binary image generation, it can be seen that the image has been split into small areas without a hair structure. Small, detached fragments below a specific pixel size were broken up, and the hair detection process was finished to remove these areas from the image. Figure 4f exhibits an example image that has been cut into little pieces.

After the hair detection step, the segmented regions on the images were filled in. In the filling process, the pixel values on the outer border of the determined regions are filled by interpolating properly inward. In inpainting section, the discrete Laplacian over the regions calculates and the Dirichlet boundary value problem solves.

### 2.3 Classification of dermoscopy images using AlexNet deep learning architecture

The transfer learning process was carried out using AlexNet [23], a convolutional neural network (CNN) based deep learning architecture that is frequently cited in the literature, to evaluate this hair removal algorithm developed in the course of the study. The AlexNet architecture was chosen because of its low computational cost compared to many other deep learning methods [17], its lower number of parameters, and the ability to apply transfer learning, which results in a shorter training time [2]. Additionally, AlexNet is capable of achieving good results even with small datasets [17] and can use images of different sizes for architecture training.

The AlexNet architecture was trained using the ISIC2018 dataset containing both raw images and the ISIC2018 dataset, which was created with the hair removal algorithm proposed and applied to hairy images in this study.

The training hyperparameters were set to use the ADAM optimization algorithm, a learning rate of 0.0001, and a minibatch size of 32, as recommended in [28]. The training was limited to 30 epochs since the training error did not decrease after 30 epochs. The training results, findings, and discussions are presented in the results and discussion section.

## 3 Results and discussion

In this study, a removal strategy for hair structures—an important morphological defect—found in dermoscopy images—the most popular imaging technique for the detection and diagnosis of skin cancers—has been provided. The main goal of algorithm is to use conventional image processing to develop a method that is more effective and requires less compute than current hair removal algorithms. The Material Method section contains information about the study in depth. This section made quantitative and qualitative assessments and compared them with previous research.

Initially, visual comparisons between the images produced by the proposed approach and the images produced by the algorithms of the research [1, 7, 18, 24, 33, 39, 41] have been exhibited in order to perform a qualitative evaluation of the images. For this, 13 images from the H13SIM and H13GAN datasets were used. Figures 5 and 6 show the images obtained from [1, 7, 18, 24, 39, 41] studies and our proposed method for the images in the H13SIM and H13GAN datasets, respectively.

When the skin lesion images obtained from the algorithms in Figs. 5 and 6 were evaluated qualitatively, it was observed that the DullRazor algorithm successfully removed hair structures in both the HairSIM and HairGAN datasets. The methods proposed by Xie et al. and Bibiloni et al. weakened the hairs in both datasets but did not completely remove them,

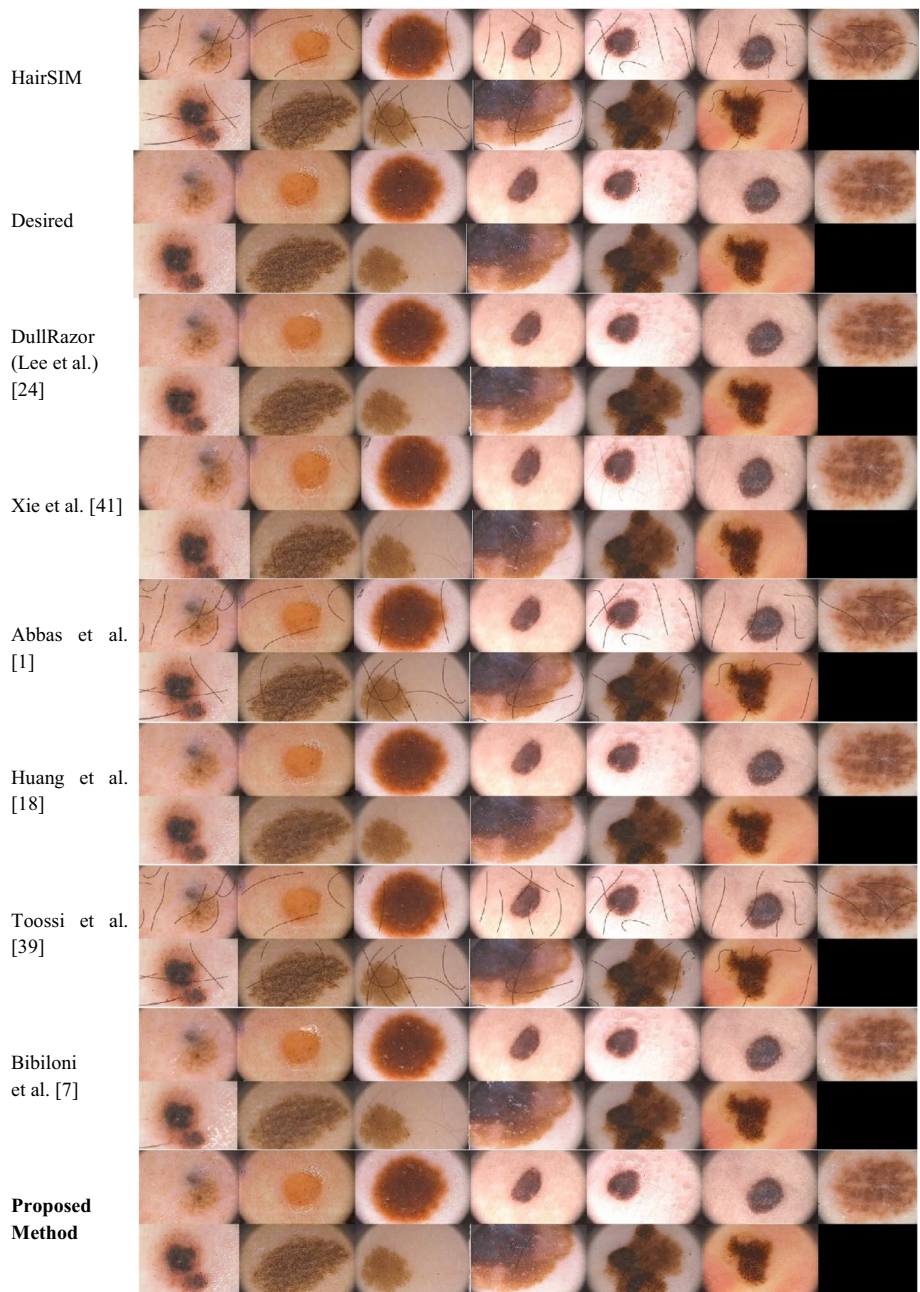


**Fig. 5** Dullrazor(Lee et al.), Xie et al., Abbas et al., Huang et al., Toosi et al., Bibiloni et al. and the results of the proposed hair removal algorithm on the H13SIM dataset

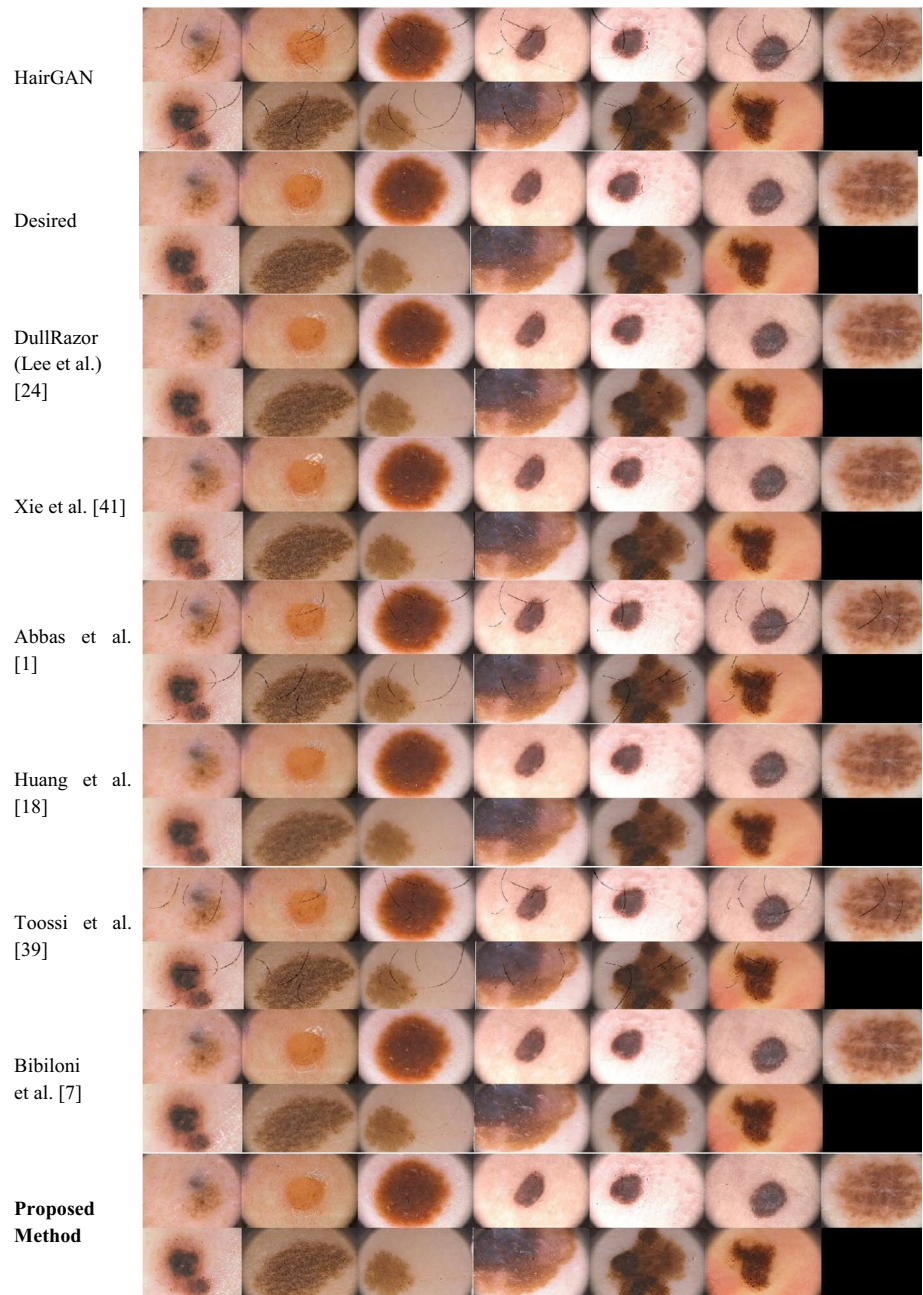


**Fig. 6** Dullrazor, Xie et al., Abbas et al., Huang et al., Toosi et al., Bibiloni et al. and the results of the proposed hair removal algorithm on the H13GAN dataset

while the methods proposed by Abbas et al. and Tossie et al. were unsuccessful in removing the hairs. The method proposed by Huang et al. was quite successful in removing hairs in the images of the HairGAN dataset but only weakened the hairs in some images of the HairSIM dataset without completely removing them. Upon careful examination of the results obtained from the proposed method in this study, it can be seen that almost all hair structures were removed, but in two images of the HairSIM dataset, a small portion of the hair structures on the lesion remained visible.

After the qualitative evaluation, the studies were evaluated quantitatively using statistical data. As seen in Tables 3 and 4, for the hairless images in the H13SIM and H13GAN datasets and the hair-removed images obtained using the hair removal algorithm, popular quality measurement metrics such as mean square error (MSE), Peak Signal-to-Noise Ratio (PSNR), Structural Similarity Index Metrics (SSIM), Mean Structural Similarity Index Metrics (MSSIM) [33, 37, 38] were calculated and were compared with other studies. Since more than one evaluation metric was used, rank analysis was performed with the obtained results and added to the tables to determine the most successful study.

The suggested algorithm appears to be in second place for the images in the HairSIM and HairGAN data sets when the rank analyses in Tables 3 and 4 are evaluated. The study of Xie et al. [41], which was largely unsuccessful in qualitative review, comes first in quantitative review. Together, the qualitative and quantitative findings demonstrate that the intended study has, on the whole, been successful. However, as indicated in Fig. 7, there are certain restrictions in the algorithm suggested in this study when it comes to removing the hairs on the skin lesions that are the same color as the skin lesions.

By modifying the algorithm parameters, the issue of weak hair structures remaining on the lesion or having colors that are similar to the lesions can be eliminated. Yet, depending on the image, this renders the proposed methodology semi-automatic. Figure 8 presents an illustration of this condition using an image from the ISIC2018 dataset.

The effectiveness of deep learning algorithms was attempted to be measured as part of the study's ongoing analysis. In this phase, the transfer learning method was utilized along with the AlexNet deep learning architecture and the ISIC2018 dataset, which included images of 7 different forms of skin cancer. In the study, the hair removal algorithm applied to both raw and processed images was deployed to train the AlexNet deep learning architecture. Table 5 lists the AlexNet deep learning architecture's performance metrics.

Looking at the results obtained in Table 5, the hair removal algorithm applied to the skin images has provided an average increase about 1% in all metrics. The results demonstrate that the hair removal algorithm to be used will enhance the success of automatic diagnosis systems. The increase in sensitivity by 1.44% indicates that the architecture detects patients more accurately. The 1% increase in F1\_score shows an increase in the rate of correctly labeling individuals as patients.

## 4 Conclusion

The hair formations that impede identification are one of the major concerns with dermoscopy images, which are frequently employed in the diagnosis of skin conditions. To enhance the precision of automatic diagnosis techniques, it is crucial to remove hair structures from images. A hair removal algorithm based on conventional image processing techniques is suggested in this study to get rid of these hair structures. Looking at the studies conducted in the literature on this problem, it is observed that deep learning methods

**Table 3** Statistical comparison results by the H13SIM data set (W1:Xie et al. [41], W2:DullRazor(Lee) et al. [24], W3:Huang et al. [18], W4:Abbas et al. [1], W5:Tossie et al. [39], W6:Bibiloni et al. [7], W7:Proposed Method)

Image	IMD006						IMD010						IMD017						IMD019					
	Studies	W7	W2	W1	W3	W6	W4	W5	W1	W7	W3	W2	W6	W4	W5	W1	W7	W3	W2	W6	W4	W5		
MSE	<b>6.34</b>	6.4	8.71	17	19.99	149.92	151.57	<b>10.4</b>	21.53	22.19	45.49	55.05	96.6	99.19	<b>9.85</b>	16.28	13.68	14.36	19.82	67.69	67.69	69.39		
PSNR	<b>40.11</b>	40.07	38.73	35.83	35.12	26.37	26.32	<b>37.96</b>	34.8	34.67	31.55	30.72	28.28	28.17	<b>38.19</b>	36.02	36.77	36.56	35.16	29.83	29.83	29.72		
SSIM	<b>0.9962</b>	0.9972	0.998	0.9932	0.9887	0.9802	0.9795	<b>0.9987</b>	0.994	0.9944	0.9929	0.9899	0.9863	0.9853	<b>0.996</b>	0.9968	0.9916	0.9916	0.9898	0.9849	0.9849	0.9834		
MSSIM	<b>0.9895</b>	0.9847	0.9727	0.9642	0.9555	0.8531	0.8483	<b>0.9805</b>	0.9854	0.9631	0.9713	0.9471	0.8953	0.888	<b>0.9878</b>	0.9863	0.9816	0.9791	0.9717	0.9343	0.9343	0.9279		
MSE R	1	2	3	4	5	6	7	1	2	3	4	5	6	7	1	4	2	3	5	6	7	7		
PSNR R	1	2	3	4	5	6	7	1	2	3	4	5	6	7	1	4	2	3	5	6	7	7		
SSIM R	3	2	1	4	5	6	7	1	3	2	4	5	6	7	2	1	4	3	5	6	7	7		
MSSIM R	1	2	3	4	5	6	7	2	1	4	3	5	6	7	1	2	3	4	5	6	7	7		
Rank	<b>6</b>	8	10	16	20	24	28	<b>5</b>	8	12	15	20	24	28	<b>5</b>	11	11	13	20	24	28	28		
Image	IMD018						IMD019						IMD020						IMD021					
	Studies	W7	W2	W3	W1	W4	W6	W5	W7	W2	W1	W3	W6	W4	W5	W1	W7	W3	W2	W6	W4	W5		
MSE	<b>5.39</b>	42.9	43.17	43.17	44.88	45.65	251.09	<b>20.98</b>	37.13	42.54	47.75	56.23	326.34	330.17	<b>7.1</b>	15.5	41.42	42.34	49.42	157.03	157.03	163.81		
PSNR	<b>40.81</b>	31.81	31.78	31.78	31.61	31.54	24.13	<b>34.91</b>	32.43	31.84	31.34	30.63	22.99	22.94	<b>39.62</b>	36.23	31.96	31.19	31.19	26.17	26.17	25.99		
SSIM	<b>0.9968</b>	0.9936	0.9935	0.9935	0.9922	0.992	0.9712	<b>0.9847</b>	0.9814	0.9865	0.9736	0.9652	0.9416	0.9372	<b>0.9976</b>	0.9904	0.9903	0.9895	0.9849	0.9717	0.9717	0.9691		
MSSIM	<b>0.994</b>	0.9674	0.9668	0.9668	0.9662	0.9644	0.8347	<b>0.987</b>	0.9661	0.9416	0.9512	0.9452	0.8163	0.8088	<b>0.9821</b>	0.9866	0.9728	0.966	0.9618	0.8703	0.8628			
MSE R	1	2	3	4	5	6	7	1	2	3	4	5	6	7	1	2	3	4	5	6	7	7		
PSNR R	1	2	3	4	5	6	7	1	2	3	4	5	6	7	1	2	3	4	5	6	7	7		
SSIM R	2	3	4	5	6	7	1	2	3	4	5	6	7	1	2	3	4	5	6	7	7	7		
MSSIM R	1	2	3	4	5	6	7	1	2	5	3	4	6	7	2	1	3	4	5	6	7	7		
Rank	<b>4</b>	8	12	16	21	23	28	<b>5</b>	9	12	15	19	24	28	<b>5</b>	7	12	16	20	24	28	28		

**Table 3** (continued)

Image	IMD030						IMD033						IMD044						IMD063					
	Studies	W1	W3	W7	W2	W6	W4	W5	W7	W3	W2	W1	W6	W4	W5	W1	W7	W4	W5	W2	W3	W6		
MSE	<b>6.16</b>	36.84	29.69	40.97	39.57	83.09	87.18	<b>12.89</b>	19.68	26.05	31.32	73.56	194.69	174.64	<b>10.18</b>	28.46	39.21	44.32	47.79	71.51	127.44			
PSNR	<b>40.23</b>	32.47	33.4	32.01	32.16	28.94	28.73	<b>37.03</b>	35.19	33.97	33.17	29.46	25.24	25.71	<b>38.05</b>	33.59	32.2	31.67	31.34	29.59	27.08			
SSIM	<b>0.9977</b>	0.9903	0.9832	0.9888	0.9871	0.9813	0.9793	<b>0.9913</b>	0.9906	0.9841	0.995	0.9719	0.9633	0.9622	<b>0.9975</b>	0.9891	0.9905	0.9885	0.9865	0.9792	0.9606			
MSSIM	<b>0.9864</b>	0.975	0.9617	0.9735	0.9672	0.9143	0.903	<b>0.9828</b>	0.964	0.9671	0.9594	0.9087	0.8628	0.8597	<b>0.9817</b>	0.9585	0.9454	0.9371	0.934	0.8866	0.8183			
MSE R	1	3	2	5	4	6	7	1	2	3	4	5	7	6	1	2	3	4	5	6	7			
PSNR R	1	3	2	5	4	6	7	1	2	3	4	5	7	6	1	2	3	4	5	6	7			
SSIM R	1	2	5	3	4	6	7	2	3	4	1	5	6	7	1	3	2	4	5	6	7			
MSSIM R	1	2	5	3	4	6	7	1	3	2	4	5	6	7	1	2	3	4	5	6	7			
Rank	<b>4</b>	10	14	16	16	24	28	<b>5</b>	10	12	13	20	26	26	<b>4</b>	9	11	16	20	24	28			
Image	IMD050						IMD061						IMD063						IMD064					
	Studies	W1	W2	W3	W6	W7	W4	W5	W1	W7	W3	W6	W2	W4	W5	W1	W7	W2	W6	W3	W4	W5		
MSE	<b>7.86</b>	21.81	11.26	40.8	94.02	122.36	121.17	<b>18.98</b>	59.6	92.93	127.41	197.82	238.37	237.68	<b>9.62</b>	11.53	60.75	63.39	65.43	89.38	95.63			
PSNR	<b>39.18</b>	34.74	37.61	32.02	28.4	27.25	27.3	<b>35.35</b>	30.38	28.45	27.08	25.17	24.36	24.37	<b>38.3</b>	37.51	30.3	30.11	29.97	28.62	28.33			
SSIM	<b>0.9977</b>	0.9954	0.995	0.9892	0.9817	0.9807	0.9806	<b>0.9938</b>	0.9721	0.9794	0.9625	0.9562	0.9347	0.9325	<b>0.9962</b>	0.9914	0.9855	0.9822	0.9815	0.9779	0.975			
MSSIM	<b>0.9718</b>	0.9848	0.976	0.9522	0.9726	0.8573	0.8563	<b>0.9741</b>	0.9712	0.9555	0.9194	0.9103	0.8199	0.8115	<b>0.9825</b>	0.9858	0.9634	0.9629	0.9573	0.9275	0.9224			
MSE R	1	3	2	4	5	7	6	1	2	3	4	5	7	6	1	2	3	4	5	6	7			
PSNR R	1	3	2	4	5	7	6	1	2	3	4	5	7	6	1	2	3	4	5	6	7			
SSIM R	1	2	3	4	5	6	7	1	3	2	4	5	6	7	1	2	3	4	5	6	7			
MSSIM R	1	2	5	3	6	7	1	1	2	3	4	5	6	7	1	2	3	4	5	6	7			
Rank	<b>7</b>	9	9	17	18	26	4	9	11	16	20	26	5	7	12	16	20	24	24	28				

**Table 3** (continued)

Image	IMD075						
		W1	W7	W6	W2	W3	W4
Studies							
MSE	<b>5.99</b>	10.17	79.01	86.17	93.96	124	132.95
PSNR	<b>40.36</b>	38.06	29.15	28.78	28.4	27.2	26.89
SSIM	<b>0.999</b>	0.9971	0.9913	0.9893	0.9873	0.9859	0.9843
MSSIM	<b>0.9856</b>	0.9897	0.9597	0.9593	0.9502	0.9051	0.8973
MSE R	<b>1</b>	2	3	4	5	6	7
PSNR R	<b>1</b>	2	3	4	5	6	7
SSIM R	<b>1</b>	2	3	4	5	6	7
MSSIM R	<b>2</b>	1	3	4	5	6	7
Rank	<b>5</b>	7	12	16	20	24	28

The bold emphasis represents the algorithm that yields the best results in the analysis of the respective table

**Table 4** Statistical comparison results by the H13GAN data set(W1:Xie et al. [41], W2:DullRazor(Lee) et al. [24], W3:Huang et al. [18], W4:Abbas et al. [1], W5:Tossie et al. [39], W6:Bibiloni et al. [7], W7:Proposed Method)

Image	IMD006						IMD010						IMD017						IMD019					
	Studies	W1	W2	W7	W3	W4	W5	W6	W7	W2	W1	W3	W4	W5	W6	W1	W7	W2	W3	W4	W5	W6		
MSE	<b>19.83</b>	20.92	23.33	33.48	64.07	62.44	4656	<b>36.3</b>	52.73	55.9	52.67	98.38	100.96	1593.6	<b>22.79</b>	24.43	24.65	35.61	67.98	68.98	3328			
PSNR	<b>35.16</b>	34.93	34.45	32.88	30.06	30.18	11.45	<b>32.53</b>	30.91	30.66	30.91	28.2	28.09	16.11	<b>34.55</b>	34.25	34.21	32.61	29.81	29.74	12.91			
SSIM	<b>0.9852</b>	0.9846	0.9875	0.9809	0.9778	0.9776	0.6705	<b>0.9876</b>	0.9827	0.9839	0.9818	0.9764	0.976	0.8675	<b>0.9778</b>	0.9816	0.9774	0.9721	0.967	0.9663	0.7697			
MSSIM	<b>0.9543</b>	0.9541	0.9434	0.918	0.9021	0.9005	0.571	<b>0.9276</b>	0.938	0.9335	0.8987	0.8835	0.8812	0.5988	<b>0.9552</b>	0.9535	0.9569	0.9301	0.9115	0.9077	0.5158			
MSE R	1	2	3	4	6	5	7	1	3	4	2	5	6	7	1	2	3	4	5	6	7			
PSNR R	1	2	3	4	6	5	7	1	3	4	2	5	6	7	1	2	3	4	5	6	7			
Rank	<b>5</b>	9	10	16	22	22	28	<b>6</b>	10	12	12	20	24	28	<b>6</b>	8	10	16	20	24	28			
Image	IMD018						IMD019						IMD020						IMD021					
	Studies	W1	W7	W2	W3	W5	W4	W6	W2	W1	W7	W4	W3	W5	W6	W1	W7	W2	W3	W4	W5	W6		
MSE	<b>23.65</b>	50.4	58.62	71.77	113.63	117.43	9149.5	<b>49.99</b>	51.37	56.15	90.7	71.58	91.59	10.911	<b>29.56</b>	45.94	61.13	69.85	132.54	139	3002.9			
PSNR	<b>34.39</b>	31.11	30.45	29.57	27.58	27.43	8.52	<b>31.14</b>	31.02	30.64	28.55	29.58	28.51	7.75	<b>33.42</b>	31.51	30.27	29.69	26.91	26.7	13.36			
SSIM	<b>0.9803</b>	0.9815	0.9767	0.9728	0.9696	0.969	0.6727	<b>0.9466</b>	0.9468	0.9426	0.9351	0.9283	0.9334	0.6023	<b>0.9694</b>	0.9755	0.965	0.9602	0.9492	0.9491	0.832			
MSSIM	<b>0.9561</b>	0.9427	0.9391	0.9122	0.9007	0.9001	0.5691	<b>0.9408</b>	0.9378	0.9249	0.9097	0.8943	0.9058	0.5075	<b>0.9566</b>	0.9432	0.9428	0.915	0.8763	0.8759	0.5345			
MSE R	1	2	3	4	5	6	7	1	2	3	5	4	6	7	1	2	3	2	3	4	5			
PSNR R	1	2	3	4	5	6	7	1	2	3	5	4	6	7	1	2	3	2	3	4	5			
SSIM R	1	2	3	4	5	6	7	1	2	3	4	6	5	7	1	2	3	2	3	4	5			
MSSIM R	1	2	3	4	5	6	7	1	2	3	4	6	5	7	1	2	3	2	3	4	5			
Rank	<b>5</b>	7	12	16	20	24	28	<b>5</b>	7	12	18	20	22	28	<b>5</b>	7	12	16	20	24	28			

**Table 4** (continued)

Image	IMD030							IMD033							IMD044							
	Studies	W1	W7	W2	W3	W4	W5	W6	W7	W1	W2	W3	W4	W5	W6	W1	W2	W4	W5	W7	W3	W6
MSE	<b>23.67</b>	38.08	57.66	57.62	76.89	79.21	1513.7	<b>26.07</b>	27.7	36.03	40.52	94.49	93.28	3308.1	<b>27.08</b>	53.35	78.29	78.67	90.26	110.18	2340.4	
PSNR	<b>34.39</b>	32.32	30.52	30.53	29.27	29.14	16.33	<b>33.97</b>	33.71	32.56	32.05	28.38	28.43	12.93	<b>33.8</b>	30.86	29.19	29.17	28.58	27.71	14.44	
SSIM	<b>0.9791</b>	0.9802	0.9714	0.9706	0.9662	0.965	0.8641	<b>0.9826</b>	0.9753	0.9695	0.97	0.9557	0.9544	0.7603	<b>0.9783</b>	0.9726	0.9683	0.9676	0.9654	0.9581	0.827	
MSSIM	<b>0.9582</b>	0.9575	0.9464	0.9311	0.9128	0.9049	0.5727	<b>0.9462</b>	0.9525	0.9459	0.9207	0.8955	0.8912	0.5076	<b>0.9626</b>	0.9303	0.9194	0.9155	0.8641	0.8183	0.4598	
MSE R	1	2	4	3	5	6	7	1	2	3	4	6	5	7	1	2	3	4	5	6	7	
PSNR R	1	2	4	3	5	6	7	1	2	3	4	6	5	7	1	2	3	4	5	6	7	
R																						
SSIM R	2	1	3	4	5	6	7	1	2	4	3	5	6	7	1	2	3	4	5	6	7	
MSSIM R	1	2	3	4	5	6	7	2	1	3	4	5	6	7	1	2	3	4	5	6	7	
R																						
Rank	<b>5</b>	<b>7</b>	<b>14</b>	<b>14</b>	<b>20</b>	<b>24</b>	<b>28</b>	<b>5</b>	<b>7</b>	<b>13</b>	<b>15</b>	<b>22</b>	<b>22</b>	<b>28</b>	<b>4</b>	<b>8</b>	<b>12</b>	<b>16</b>	<b>20</b>	<b>24</b>	<b>28</b>	
Image	IMD050							IMD061							IMD063							
	Studies	W7	W1	W2	W3	W4	W5	W6	W7	W1	W2	W3	W4	W5	W6	W1	W2	W4	W5	W7	W3	W6
MSE	<b>18.97</b>	28.81	41.72	29.14	55.62	55.45	2353.2	<b>39.24</b>	82.7	125.81	206.68	170.74	168.47	4311	<b>23.19</b>	68.48	78.06	81.6	87.61	82.45	9168.7	
PSNR	<b>35.35</b>	33.53	31.93	33.49	30.68	30.69	14.41	<b>32.19</b>	28.96	27.13	24.98	25.81	25.87	11.78	<b>34.48</b>	29.78	29.21	29.01	28.71	28.97	8.51	
SSIM	<b>0.9872</b>	0.9775	0.9754	0.9764	0.9721	0.9717	0.7209	<b>0.9508</b>	0.9598	0.9552	0.9232	0.9072	0.9061	0.6682	<b>0.9608</b>	0.9638	0.9505	0.9439	0.946	0.9435	0.6692	
MSSIM	<b>0.9533</b>	0.9532	0.9542	0.9542	0.9295	0.906	0.9046	0.5122	<b>0.947</b>	0.9379	0.9067	0.891	0.8393	0.8342	0.5206	<b>0.9547</b>	0.9425	0.9336	0.9095	0.912	0.9107	0.565
MSE R	1	2	4	3	6	5	7	1	2	3	6	5	4	7	1	2	3	4	6	5	7	
PSNR R	1	2	4	3	6	5	7	1	2	3	6	5	4	7	1	2	3	4	6	5	7	
R																						
SSIM R	2	1	4	3	5	6	7	1	2	3	4	5	6	7	1	2	3	5	4	6	7	
MSSIM R	3	1	4	5	6	7	1	2	3	4	5	6	7	1	2	3	6	4	5	7		
R																						
Rank	<b>5</b>	<b>9</b>	<b>13</b>	<b>13</b>	<b>22</b>	<b>22</b>	<b>28</b>	<b>5</b>	<b>7</b>	<b>12</b>	<b>20</b>	<b>20</b>	<b>20</b>	<b>28</b>	<b>5</b>	<b>7</b>	<b>12</b>	<b>19</b>	<b>20</b>	<b>21</b>	<b>28</b>	

**Table 4** (continued)

Image	IMD075					
	Studies	W1	W5	W7	W4	W2
MSE	<b>29.23</b>	80.6	96.78	82.11	107.53	122.34
PSNR	<b>33.47</b>	29.07	28.27	28.99	27.82	27.26
SSIM	<b>0.9876</b>	0.9794	0.9798	0.9793	0.9792	0.9757
MSSIM	<b>0.9507</b>	0.9172	0.9185	0.9185	0.9234	0.8889
MSE R	<b>1</b>	2	4	3	5	6
PSNR R	<b>1</b>	2	4	3	5	7
SSIM R	<b>1</b>	3	2	4	5	6
MSSIM R	<b>1</b>	5	3	4	2	6
R						
Rank	<b>4</b>	12	13	14	17	24
						28

The bold emphasis represents the algorithm that yields the best results in the analysis of the respective table



**Fig. 7** Hair structures that the algorithm cannot remove

provide more successful results compared to morphological image processing methods in hair removal techniques. However, an automatic skin cancer detection system already uses a deep learning architecture for classification. Adding a new deep learning architecture to the system only for removing hair structures will increase the computational cost. Therefore, in this study, a hair removal algorithm has been proposed using traditional morphological image processing methods. The proposed algorithm is based on the top-hat algorithm, which highlights small details and structures, brightness of dark areas or details in the background, and flat-field correction operations.

Qualitative and quantitative evaluation were utilized to compare the method to other hair removal algorithms in the literature. In the qualitative evaluations, hair removal images, which are among the successful studies, took the 2nd place in the quantitative evaluation order. It is seen that the study, which ranks 1st in the quantitative comparison tables and proposed by Xie et al. [41], did not provide successful results in removal of hair in the context of qualitative evaluation. For this reason, as the qualitative and quantitative evaluation results of the algorithm in this study are taken together, it is observed that it holds the first position among algorithms based on traditional methods. In the following part of the study, raw and hair removal algorithms have been administered in order to observe the performance of hair removal algorithms on automatic diagnosis methods, and classification performances of AlexNet deep learning architecture trained with images have been compared. The reason why AlexNet architecture was selected in this study is that it has low

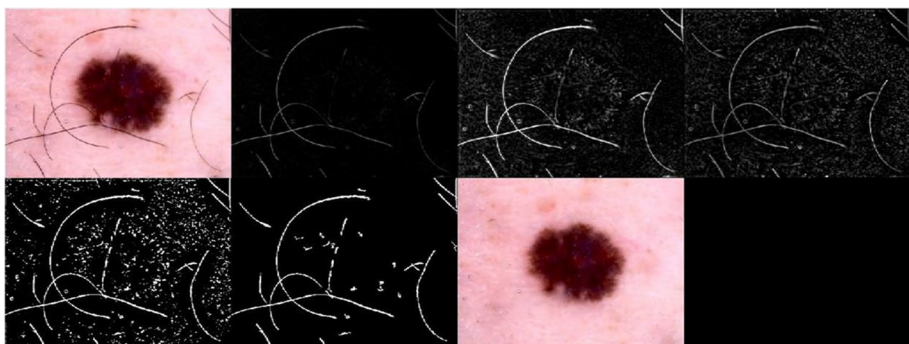


**Fig. 8** Removal of hair structures on the lesion

**Table 5** Classification results of the AlexNet architecture for ISIC-2018 data set

	Accuracy	Sensitivity	Specificity	Precision	F1_score
Hair Removal Applied Images	0.71758	0.72213	0.95224	0.74128	0.72312
Raw Images	0.70861	0.70776	0.95064	0.73516	0.71252

computational cost, it trains relatively fast compared to other deep learning methods, and it revealed successful results in previous studies on skin cancer diagnosis. Containing images of 7 different skin cancer types, the ISIC2018 dataset was used and the hair removal algorithm was used after the training. The trained architecture showed up to 1% better results than the trained architecture with raw images.

It is argued that higher quality dermoscopy images made possible by the proposed hair removal technique can enhance the segmentation and classification of skin lesion research. It is believed that doing so will enable the development of computer-aided diagnosis systems with improved performance. Further, this can help professionals make decisions during consultations. Given the algorithm's limitations, it can be seen that the algorithm struggles to tell apart hair structures that share the same color tones as the lesion on the lesion images. Future research may employ a wide range of approaches to address this issue. On the other hand, even if the hair structure is the main issue with skin lesions, there may be many morphological defects (markings, water spots, white spots, etc.). Future research could concentrate on removing other morphological deficiencies in images with deconstructed hair structures. Looking at it from another perspective, deep learning methods have been shown to be successful in removing noise from images. However, using a deep learning architecture solely for noise reduction would add extra computational cost to automatic diagnosis systems. Therefore, future studies could aim to find an optimal solution by using a single deep learning architecture for both denoising dermoscopy images and performing segmentation.

**Data Availability** The data that support the findings of this study are available in ISIC2018 and Dermaweb, reference number [10], [15] and [40]. These data were derived from the following resources available in the public domain: ISIC2018, <https://challenge.isic-archive.com/data/#2018>; Dermaweb, <http://dermaweb.uib.es/hair-removal-benchmarks/>.

## Declarations

**Competing interest** The authors declare that they have no known competing financial interests or personal relationships that could have appeared to influence the work reported in this paper.

## References

1. Abbas Q, Celebi ME, García IF (2011) Hair removal methods: a comparative study for dermoscopy images. *Biomed Signal Process Control* 6:395–404. <https://doi.org/10.1016/j.bspc.2011.01.003>
2. Ariff NAM, Ismail AR (2023) Study of Adam and Adamax optimizers on AlexNet architecture for voice biometric authentication system. *Proc 2023 17th Int Conf Ubiquitous Inf Manag Commun IMCOM 2023*. <https://doi.org/10.1109/IMCOM56909.2023.10035592>
3. Arora G, Dubey AK, Jaffery ZA, Rocha A (2022) A comparative study of fourteen deep learning networks for multi skin lesion classification (MSLC) on unbalanced data. *Neural Comput Appl* 1–27. <https://doi.org/10.1007/S00521-022-06922-1>

4. Attia M, Hossny M, Nahavandi S, Yazdabadi A (2017) Skin melanoma segmentation using recurrent and convolutional neural networks. *Proc - Int Symp Biomed Imaging*, pp 292–296. <https://doi.org/10.1109/ISBI.2017.7950522>
5. Attia M, Hossny M, Zhou H et al (2019) Digital hair segmentation using hybrid convolutional and recurrent neural networks architecture. *Comput Methods Programs Biomed* 177:17–30. <https://doi.org/10.1016/J.CMPB.2019.05.010>
6. Berry K, Butt M, Kirby JS (2017) Influence of information framing on patient decisions to treat actinic keratoses. *JAMA Dermatol* 153:421–426. <https://doi.org/10.1001/JAMADERMATOL.2016.5245>
7. Bibiloni P, González-Hidalgo M, Massanet S (2017) Skin hair removal in dermoscopic images using soft color morphology. *Lect Notes Comput Sci (including Subser Lect Notes Artif Intell Lect Notes Bioinformatics)*, pp 322–326. [https://doi.org/10.1007/978-3-319-59758-4\\_37](https://doi.org/10.1007/978-3-319-59758-4_37)
8. Brantsch KD, Meisner C, Schönfisch B et al (2008) Analysis of risk factors determining prognosis of cutaneous squamous-cell carcinoma: a prospective study. *Lancet Oncol* 9:713–720. [https://doi.org/10.1016/S1470-2045\(08\)70178-5](https://doi.org/10.1016/S1470-2045(08)70178-5)
9. Chadebec C, Thibeau-Sutre E, Burgos N, Allassonniere S (2023) Data augmentation in high dimensional low sample size setting using a geometry-based variational autoencoder. *IEEE Trans Pattern Anal Mach Intell* 45:2879–2896. <https://doi.org/10.1109/TPAMI.2022.3185773>
10. Codella NCF, Gutman D, Celebi ME et al (2018) Skin lesion analysis toward melanoma detection: a challenge at the 2017 International symposium on biomedical imaging (ISBI), hosted by the international skin imaging collaboration (ISIC). *Proc - Int Symp Biomed Imaging*, pp 168–172. <https://doi.org/10.1109/ISBI.2018.8363547>
11. Davidson DW, Fröjd C, O'Shea V et al (2003) Limitations to flat-field correction methods when using an X-ray spectrum. *Nucl Instruments Methods Phys Res Sect A Accel Spectrometers, Detect Assoc Equip* 509:146–150. [https://doi.org/10.1016/S0168-9002\(03\)01563-8](https://doi.org/10.1016/S0168-9002(03)01563-8)
12. Gao J, Pan JH, Zhang SJ, Zheng WS (2023) Automatic modelling for interactive action assessment. *Int J Comput Vis* 131:659–679. <https://doi.org/10.1007/S11263-022-01695-5>
13. Gaulin C, Sebaratnam DF, Fernández-Peña P (2014) Quality of life in non-melanoma skin cancer. *Australas J Dermatol* 56:70–76. <https://doi.org/10.1111/AJD.12205>
14. Hasan MK, Elahi MTE, Alam MA et al (2022) DermoExpert: skin lesion classification using a hybrid convolutional neural network through segmentation, transfer learning, and augmentation. *Informatics Med Unlocked* 28:100819. <https://doi.org/10.1016/J.IMU.2021.100819>
15. Home | DermaWeb. <http://dermaweb.uib.es/>. Accessed 13 Jun 2022
16. Hosny KM, Kassem MA (2022) Refined residual deep convolutional network for skin lesion classification. *J Digit Imaging* 35:258–280. <https://doi.org/10.1007/S10278-021-00552-0>
17. Hosny KM, Kassem MA, Foaud MM (2019) Classification of skin lesions using transfer learning and augmentation with Alex-net. *PLoS One* 14:e0217293. <https://doi.org/10.1371/JOURNAL.PONE.0217293>
18. Huang A, Kwan SY, Chang WY et al (2013) A robust hair segmentation and removal approach for clinical images of skin lesions. *Proc Annu Int Conf IEEE Eng Med Biol Soc EMBS*, pp 3315–3318. <https://doi.org/10.1109/EMBC.2013.6610250>
19. Karia PS, Han J, Schmults CD (2013) Cutaneous squamous cell carcinoma: estimated incidence of disease, nodal metastasis, and deaths from disease in the United States, 2012. *J Am Acad Dermatol* 68:957–966. <https://doi.org/10.1016/J.JAAD.2012.11.037>
20. Kassem MA, Hosny KM, Damaševičius R, Eltoukhy MM (2021) Machine learning and deep learning methods for skin lesion classification and diagnosis: a systematic review. *Diagnostics* 11:1390. <https://doi.org/10.3390/DIAGNOSTICS11081390>
21. Kiani K, Sharafat AR (2011) E-shaver: an improved DullRazor® for digitally removing dark and light-colored hairs in dermoscopic images. *Comput Biol Med* 41:139–145. <https://doi.org/10.1016/J.COMBIOMED.2011.01.003>
22. Koehoorn J, Sobiecki AC, Boda D et al (2015) Automated digital hair removal by threshold decomposition and morphological analysis. *Lect Notes Comput Sci (including Subser Lect Notes Artif Intell Lect Notes Bioinformatics)* 9082:15–26. [https://doi.org/10.1007/978-3-319-18720-4\\_2](https://doi.org/10.1007/978-3-319-18720-4_2)
23. Krizhevsky A, Sutskever I, Hinton GE (2017) ImageNet classification with deep convolutional neural networks. *Commun ACM* 60:84–90. <https://doi.org/10.1145/3065386>
24. Lee T, Ng V, Gallagher R et al (1997) Dullrazor®: a software approach to hair removal from images. *Comput Biol Med* 27:533–543. [https://doi.org/10.1016/S0010-4825\(97\)00020-6](https://doi.org/10.1016/S0010-4825(97)00020-6)
25. Leiter U, Eigenthaler T, Garbe C (2014) Epidemiology of skin cancer. *Adv Exp Med Biol* 810:120–140. [https://doi.org/10.1007/978-1-4939-0437-2\\_7](https://doi.org/10.1007/978-1-4939-0437-2_7)
26. Li W, Joseph Raj AN, Tjahjadi T, Zhuang Z (2021) Digital hair removal by deep learning for skin lesion segmentation. *Pattern Recognit* 117:107994. <https://doi.org/10.1016/J.PATCOG.2021.107994>

27. Mahbod A, Schaefer G, Wang C et al (2020) Transfer learning using a multi-scale and multi-network ensemble for skin lesion classification. *Comput Methods Programs Biomed* 193:105475. <https://doi.org/10.1016/j.cmpb.2020.105475>
28. Mat Ariff NA, Ismail AR, Aziz NA, Amir Hussin AA (2022) Analysis of optimizers on AlexNet architecture for face biometric authentication system. 2022 Int Conf Inf Technol Res Innov ICITRI 2022, pp 24–29. <https://doi.org/10.1109/ICITRI56423.2022.9970238>
29. Mathews MR, Anzar SM (2021) A comprehensive review on automated systems for severity grading of diabetic retinopathy and macular edema. *Int J Imaging Syst Technol* 31:2093–2122. <https://doi.org/10.1002/IMA.22574>
30. Model MA, Burkhardt JK (2001) A standard for calibration and shading correction of a fluorescence microscope. *J Quant Cell Sci* 44:309–316. [https://doi.org/10.1002/1097-0320\(20010701\)44:3%3c179::AID-CYTO1110%3e3.0.CO;2-3](https://doi.org/10.1002/1097-0320(20010701)44:3%3c179::AID-CYTO1110%3e3.0.CO;2-3)
31. Otsu N (1979) A threshold selection method from gray-level histograms. *IEEE Trans Syst Man Cybern* 9:62–66. <https://doi.org/10.1109/tsmc.1979.4310076>
32. Pereira PMM, Fonseca-Pinto R, Paiva RP et al (2020) Dermoscopic skin lesion image segmentation based on local binary pattern clustering: comparative study. *Biomed Signal Process Control* 59:101924. <https://doi.org/10.1016/j.bspc.2020.101924>
33. Ramella G (2021) Hair removal combining saliency, shape and color. *Appl Sci* 11:447. <https://doi.org/10.3390/APP11010447>
34. Seibert JA, Boone JM, Lindfors KK (1998) Flat-field correction technique for digital detectors. *Med Imaging 1998 Phys Med Imaging* 3336:348–354. <https://doi.org/10.1117/12.317034>
35. Siegel RL, Miller KD, Fuchs HE, Jemal A (2022) Cancer statistics. *CA Cancer J Clin* 72:7–33. <https://doi.org/10.3322/CAAC.21708>
36. Smith L, MacNeil S (2011) State of the art in non-invasive imaging of cutaneous melanoma. *Ski Res Technol* 17:257–269. <https://doi.org/10.1111/J.1600-0846.2011.00503.X>
37. Süzme NÖ, Gürakşin GE (2020) Comparison of image quality measurements in threshold determination of most popular gradient based edge detection algorithms based on particle swarm optimization. *Lect Notes Data Eng Commun Technol* 43:171–181. [https://doi.org/10.1007/978-3-030-36178-5\\_14](https://doi.org/10.1007/978-3-030-36178-5_14)
38. Talavera-Martínez L, Bibiloni P, González-Hidalgo M (2020) An encoder-decoder CNN for hair removal in dermoscopic images. *ArXiv*. <https://doi.org/10.48550/arxiv.2010.05013>
39. Toossi MTB, Pourreza HR, Zare H et al (2013) An effective hair removal algorithm for dermoscopy images. *Ski Res Technol* 19:230–235. <https://doi.org/10.1111/SRT.12015>
40. Tschandl P, Rosendahl C, Kittler H (2018) Data descriptor: the HAM10000 dataset, a large collection of multi-source dermatoscopic images of common pigmented skin lesions. *Sci Data* 5:1–9. <https://doi.org/10.1038/sdata.2018.161>
41. Xie FY, Qin SY, Jiang ZG, Meng RS (2009) PDE-based unsupervised repair of hair-occluded information in dermoscopy images of melanoma. *Comput Med Imaging Graph* 33:275–282. <https://doi.org/10.1016/J.COMPMEDIMAG.2009.01.003>
42. Xie F, Li Y, Meng R, Jiang Z (2015) No-reference hair occlusion assessment for dermoscopy images based on distribution feature. *Comput Biol Med* 59:106–115. <https://doi.org/10.1016/J.COMPBIMED.2015.01.023>
43. Yu Z, Ge Z, Nguyen J et al (2022) Early melanoma diagnosis with sequential dermoscopic images. *IEEE Trans Med Imaging* 41:633–646. <https://doi.org/10.1109/TMI.2021.3120091>
44. Zheng X, Sun H, Lu X, Xie W (2022) Rotation-invariant attention network for hyperspectral image classification. *IEEE Trans Image Process* 31:4251–4265. <https://doi.org/10.1109/TIP.2022.3177322>
45. Zhu H, Liu S, Deng L et al (2020) Infrared small target detection via low-rank tensor completion with top-hat regularization. *IEEE Trans Geosci Remote Sens* 58:1004–1016. <https://doi.org/10.1109/TGRS.2019.2942384>

**Publisher's note** Springer Nature remains neutral with regard to jurisdictional claims in published maps and institutional affiliations.

Springer Nature or its licensor (e.g. a society or other partner) holds exclusive rights to this article under a publishing agreement with the author(s) or other rightsholder(s); author self-archiving of the accepted manuscript version of this article is solely governed by the terms of such publishing agreement and applicable law.